

# Extraordinary Activity in the BL Lac Object OJ 287

Philip A. Hughes, Hugh D. Aller and Margo F. Aller

Astronomy Department, University of Michigan, Ann Arbor, MI 48109-1090;  
hughes@astro.lsa.umich.edu, hugh@astro.lsa.umich.edu, margo@astro.lsa.umich.edu

## ABSTRACT

We use a continuous wavelet transform to analyze more than two decades of data for the BL Lac object OJ 287 acquired as part of the UMRAO variability program. We find clear evidence for a persistent modulation of the total flux and polarization with period  $\sim 1.66$  years, and for another signal that dominates activity in the 1980s with period  $\sim 1.12$  years. The relationship between these two variations can be understood in terms of a ‘shock-in-jet’ model, in which the longer time scale periodicity is associated with an otherwise quiescent jet, and the shorter time scale activity is associated with the passage of a shock; the different periodicities of these two components may reflect different internal conditions of the two flow domains, leading to different wave speeds, or different contractions of a single underlying periodicity, due to the different Doppler factors of the two flow components. We suggest that the modulation arises from a wave driven by some asymmetric disturbance close to the central engine. The periodic behavior in polarization exhibits excursions in  $U$  which correspond to a direction  $\sim 45^\circ$  from the VLBI jet axis. This behavior is not explained by the random walk in the  $Q$ - $U$  plane which is expected from models in which a pattern of randomly aligned magnetic field elements propagate across the visible portion of the flow, and suggests a small amplitude, cyclic variation in the flow direction in that part of the flow that dominates cm-wavelength emission.

*Subject headings:* BL Lacertae objects: individual (OJ 287) — galaxies: active — galaxies: jets — polarization — shock waves

## 1. Introduction

It is generally accepted that centimeter-waveband emission from AGNs is associated with a jet of synchrotron plasma, the accretion structure and immediate environment of the central supermassive black hole contributing broadband emission from the infrared

to  $\gamma$ -rays (e.g., Bregman 1994). A number of processes may be responsible for temporal variations in the radio flux: the fueling (accretion) rate may change with time, leading to a long-term change in the jet power; the accretion disk may exhibit instability, influencing the extraction of energy in the form of a collimated outflow; the outflow itself may be Kelvin-Helmholtz unstable, leading to propagating internal structures (e.g. shocks); the outflow may interact with ambient inhomogeneities, which also may produce disturbances to the body of the flow (Wiita 1991; Birkinshaw 1991; Icke 1991). However, while there can be characteristic time scales associated with all such process, there is no a priori reason to believe that such variations will be *periodic*. Nevertheless, a detailed understanding of blazars demands a detailed description of the temporal variations, which for completeness requires a search for periodicity.

OJ 287 is a BL Lac object with  $z = 0.306$  (Miller, French, & Hawley 1978; Sitko & Junkkarinen 1985), whose behavior differs in a number of intriguing ways from that of other blazars. Large amplitude, short time scale variations (Sillanpää et al. 1994; Kidger & González-Pérez 1994; Valtaoja, Teräsanta, & Tornikoski 1994; Aller, Aller, & Hughes 1994) are seen in the light curves from the radio to optical wavebands. In the optical waveband, OJ 287 displays activity down to a time scale  $\sim 10$  minutes (Boltwood 1996). Numerous periodicities have been claimed, the strongest evidence being for a period  $\sim 12$  yr evident in optical data that span more than one century (Sillanpää et al. 1988). This period has been interpreted by Valtonen and coworkers (e.g., Valtonen & Lehto 1997) as being due to the passage of the secondary black hole of a binary system through the accretion disk of the primary black hole. Interpreting VLB polarization observations in the context of a ‘shock-in-jet model’, Cawthorne & Wardle (1988) suggests that the radio jet is aligned very close to the critical cone,  $\theta_c = \sin^{-1}(1/\gamma)$ , in contrast with viewing angles of tens of degrees suggested by the modelling of events in some blazars (Hughes, Aller, & Aller 1989, 1991; Mutel et al. 1990; Carrara et al. 1993). This suggests that the flow should have a Doppler factor significantly in excess of unity, with a concomitant reduction in observed time scales – making the source uniquely suited for an analysis of periodicity, because of the many cycles observed. Indeed, Katz (1997) has proposed a model based on a precessing disk, that would demand an extremely high Lorentz factor ( $\sim 50$ ), and thus a high Doppler factor if the flow is seen from close to, or within, the critical cone.

Motivated by the preceding arguments, and by the intriguing claims of periodicity for the optical light curve of OJ 287, we performed a number of spectral analyses of centimeter waveband data for those sources well-enough observed to justify a structure function analysis (Hughes, Aller, & Aller 1992). Both Deeming (1975) and Scargle (1982) periodograms were constructed, together with smoothed power spectra using both standard tapering and smoothing techniques (Jenkins & Watts 1968), and a maximum entropy

approach (Haykin & Kesler 1979; Ulrych & Ooe 1979). In general, each source exhibited a complex distribution of power with frequency, due in part to the fact that most activity is aperiodic, and in part to the observing window. In only one source – OJ 287 – was there some evidence for periodicity; in that case the Scargle false-alarm probability gave us some confidence in a variation with time scale  $\sim 1.6$  yr (Aller, Aller, Hughes, & Latimer 1992).

Although a powerful technique in the right context, the fundamental limitation of Fourier methods is that they do not preserve the temporal locality of a signal. Power associated with the data’s window will appear at low frequencies, possibly near to the frequency of a sought periodic signal, while outbursts with a character that is certainly not periodic will place power across the spectrum. Identifying periodicity that is well-hidden by other variations requires assessing the significance of one, among many, peaks in the power spectrum. A method of analysis that circumvents this problem is continuous wavelet analysis, which we discuss in detail in § 3. For a one-dimensional data set such as a time series, a wavelet analysis amounts to quantifying the behavior of the signal on different temporal scales, as a function of time. This is achieved by convolving the signal with a localized wave-packet, as the packet is translated along the series, for a number of ‘dilations’ of the wave-packet, i.e., for progressively broader wave-packets, sensitive to progressively longer time scale behavior. Thus an initially narrow wave-form, sensitive to high frequency structure in the signal, is progressively stretched, or dilated, in time, making it sensitive to lower frequency structure. We are currently exploring the behavior exhibited by various sources in the UMRAO database using continuous wavelets, and here report results for OJ 287, having chosen this source as the first to study in light of its unique character.

## 2. Centimeter Waveband Data

Figure 1 shows the UMRAO data for OJ 287 averaged in 30-day periods to reduce the crowding of data points. Observations were made at approximately weekly intervals at each frequency starting in 1978, 1971 and 1974 at 4.8, 8.0 and 14.5 GHz respectively. There is a systematic gap in the data at yearly intervals (of approximately 30-day duration) to avoid solar interference when the sun is too close to the source. There are other gaps of varying length in the data, due to bad weather and equipment malfunctions, but these are randomly placed throughout the observing period. Selected HII regions, Galactic supernova remnants and radio galaxies were observed each day to determine the effective collecting area of the telescope and to verify the stability of the instrumental polarization. The observing technique and data reduction procedures are discussed more fully by Aller et al. (1985, 1997). The wavelet analysis that follows uses the unaveraged data: 583 points at 4.8 GHz,

1060 points at 8.0 GHz and 828 points at 14.5 GHz.

### 3. The Continuous Wavelet Transform

The fundamental concept behind continuous wavelet analysis is to convolve the ‘signal’ under study with a translated and dilated ‘mother’ wavelet, in order to map out in translation-dilation space the power in a signal at a particular time, on a particular scale. The great advantage of this over Fourier techniques is the preservation of temporal locality: a gap in the time series will be evident along the corresponding line in transform space, and events that are distinct in the signal will have distinct counterparts in transform space. A corollary of this is that there is a redundancy in the wavelet transform of a periodic signal – a set of peaks and troughs in the real part of the transform, that ‘march’ across transform space at fixed dilation – that makes the detection of periodicity very easy. A number of reviews and books addressing this subject have appeared since the early 1990s; we follow here a review by Farge (1992) on the application of wavelet analysis to the study of turbulence.

The Morlet wavelet has been extensively used in a number of fields of study, and it has the advantage of being both complex and progressive. Being complex, the real part of the transform exhibits an oscillatory behavior corresponding to periodicity of the signal being analyzed, thus highlighting such periodic behavior, while we can construct the modulus, which because of the phase shift between the real and imaginary parts of the wavelet coefficients, provides a smooth estimation of the power in the signal being analyzed, and its temporal persistence. The frequency of a periodic signal may be read from the phase plot, which also provides a sensitive diagnostic of both changes in characteristic behavior of the signal and sharp pulses. Being progressive, i.e., having zero power at negative frequency, the wavelet is optimal for the analysis of causal signals, because it does not admit an interference between the past and future parts of the signal at any instant in the time series. The wavelet is characterized by a frequency  $\omega_\psi$ :

$$\psi_{\text{Morlet}} = e^{-i\omega_\psi t} e^{-|t|^2/2}, \quad (1)$$

and has Fourier transform

$$\hat{\psi}(\omega) = (2\pi)^{-1} \int_{\mathbf{R}} \psi(\mathbf{t}) e^{-i\omega t} dt, \quad (2)$$

given by

$$\hat{\psi}(\omega) = \begin{cases} (2\pi)^{-1/2} e^{-(\omega-\omega_\psi)^2/2} & \text{if } \omega > 0; \\ 0 & \text{if } \omega \leq 0. \end{cases} \quad (3)$$

To provide a good resolution of temporal structures we want to choose  $\omega_\psi$  to be small (the higher the frequency of the analyzing wavelet, the greater the extent to which the wavepacket is a broad oscillatory structure, which ‘delocalizes’ structure in the signal, as does Fourier transformation – just what we are trying to avoid); however, the mother wavelet must satisfy an admissibility condition

$$C_\psi = (2\pi) \int_{\mathbf{R}} |\hat{\psi}(\omega)|^2 \frac{d\omega}{\omega} < \infty. \quad (4)$$

Equation (4) is equivalent to requiring a zero mean:

$$\int_{\mathbf{R}} \psi(t) dt = 0. \quad (5)$$

This condition is not formally satisfied by the wavelet of equation (1) for any value of  $\omega_\psi$ ; however if  $\omega_\psi$  is large enough, the admissibility condition is satisfied to the single precision machine accuracy with which wavelet coefficients are computed. A value of  $\omega_\psi = 5$  reconciles the conflicting requirements of resolution and admissibility; we have performed the analysis described below with different values of  $\omega_\psi$ , with no discernible change in the transform coefficients.

Having selected a mother wavelet, the wavelet coefficients are found by constructing a set of translated ( $t'$ ) and dilated ( $l$ ) wavelets

$$\psi_{lt'}(t) = l^{-1/2} \psi \left[ \frac{t - t'}{l} \right], \quad l \in \mathbf{R}^+, \quad t \in \mathbf{R}, \quad (6)$$

and convolving with the signal:

$$\tilde{f}(l, t') = \int_{\mathbf{R}} f(t) \psi_{lt'}^*(t) dt. \quad (7)$$

We have chosen to normalize so that all wavelets have the same  $L^2$  norm so that wavelet coefficients correspond to energy densities. The discrete nature of the data, of course, means that the above integrals have to be approximated as sums, and we evaluate  $\tilde{f}(l, t')$  on a mesh of values  $(l_i, t'_i)$ , fine enough to display all the structure associated with the input signal. The data are well-sampled with an *approximately* constant density of sampling points on time scales significantly shorter than that of the spectral features discussed here, and contain few gaps. To facilitate the computations, we interpolate the data onto a uniform sampling grid with scale  $\Delta t$ , and compute the wavelet coefficients up to a dilation  $l_{\max}$  corresponding to a time scale of 5 years. The interpolation has no significant influence on the signal for structures with scale  $\gg \Delta t$ . The convolution that determines the wavelet coefficients  $\tilde{f}(l, t')$  requires data within a domain of influence  $t' - l \lesssim t \lesssim t' + l$ , and so the

larger the dilation,  $l$ , the further does the effect of the ends of the time series extend. The conservative choice of a 5 year limit ensures good coverage of transform space unpolluted by edge effects. In the transform space plots shown below we have masked out the wavelet coefficients within  $1.5l$  of the boundaries, the domain in which the coefficients cannot be reliably computed. Note that these plots are linear in translation, and logarithmic in dilation.

As examples of this technique, Figures 2a and 2b show the transforms of Gaussian white noise and a sinusoidal signal in which the frequency halves at the mid-point of the time series respectively. A short period of ‘coherent’ activity in the white noise signal leads to structure in the real part of the transform coefficients that might be mistaken for periodicity. Examination of the modulus, however, shows that this feature is transitory.

The admissibility condition guarantees that the wavelet coefficients may be used to reconstruct the original signal:

$$f(t) = C_\psi^{-1} \int_{\mathbf{R}} \int_{\mathbf{R}^+} \tilde{f}(l, t') \psi_{lt'}(t) \frac{dl dt'}{l^2}, \quad (8)$$

and the fact that nearby wavelet coefficients are correlated corresponds to a redundancy in the set of coefficients  $\tilde{f}(l, t')$  which means that a wavelet different from the analyzing wavelet may be used in the reconstruction; in fact, a delta distribution may be used, leading to the simple reconstruction formula

$$f(t) = C_\delta^{-1} \int_{\mathbf{R}^+} \tilde{f}(l, t) \frac{dl}{l^{1+(1/2)}}, \quad (9)$$

where

$$C_\delta = (2\pi)^{1/2} \int_{\mathbf{R}} \hat{\psi}(\omega) \frac{d\omega}{\omega}. \quad (10)$$

We cannot reconstruct the original signal exactly because we compute the transform coefficients for only a finite set of translations and dilations. In particular, the upper bound on  $l$  implies that the wavelet coefficients contain no information about long-term trends (beyond about 5 yr), and effectively subtracts a local mean. The main purpose of reconstruction is to display that part of the signal within limited ranges of  $l$ ; we can assess the validity of that by comparing the reconstruction that uses all available dilations with the original signal. Use of a discrete transform in which the analyzing wavelets form a complete orthogonal basis (Farge 1992) would provide the ability to invert exactly, but the continuous transform used here provides a much more useful method for illuminating the nature of the signal variations, and in particular highlighting periodicities.

## 4. Analysis of the Total Flux Variations

### 4.1. The Transform Coefficients

Figure 3 shows the Morlet transform for the 14.5 GHz flux data for OJ 287. Some power is evident over the whole range of time scales explorable within the time series, but the most obvious feature is the signature of periodicity at low frequency, in the form of a pattern of peaks and troughs that crosses the transform plane at fixed dilation. This pattern is modified during the 1980s, by the appearance of shorter period activity, but resumes after the latter activity has subsided. Evidently this shorter period activity results from a coexisting emission component, because both signals may be seen distinctly at some epochs, e.g., 1983, and hints of the shorter period activity persist into the 1990s. The transforms of the 8.0 and 4.8 GHz data are similar to the one shown. However, the interpretation of the 4.8 GHz transform is somewhat less clear-cut because of structure in transform space on the longest time scales accessible to study; this presumably results from the fact that at the lowest observing frequency we are including contributions from larger scale flows (Marscher 1993). For comparison, Figures 4a and 4b show the transforms of two sources observed in the Michigan program that do not exhibit the periodic type of activity seen in OJ 287. A short period of ‘coherent’ activity in the major outburst seen in BL Lac in the early 1980s leads to structure in the real part of the transform coefficients that might be mistaken for periodicity. Examination of the modulus, however, shows that this feature is transitory, and quite different from the persistent modulation seen in OJ 287. There is a hint of periodic behavior in NRAO 140, seen in the real part of the transform coefficients at the longest dilation, between the mid-1980s and mid-1990s, but on time scales too long to be explored with the current data.

To assess the probability that the transform of OJ 287 is significantly different from that of Gaussian white noise, we have computed a  $\chi^2$ -statistic based on a pixel-by-pixel comparison of the two transforms. As we are concerned with a comparison of the large amplitude structures evident at high dilations, and also wish to judge the validity of a model presented in §4.2 – which makes no attempt to fit the low level structure of the upper half transform plane, we have used the standard deviation of the transform modulus in the upper half plane as an estimate of an ‘error’ in the OJ 287 transform. We find a  $\chi^2$  probability of  $\sim 100\%$  that the model discussed below fits the data, but a probability of  $\lesssim 10^{-5}\%$  (i.e., zero to machine accuracy) that Gaussian white noise can model the data, for a number of realizations of a noise-based signal.

The frequency of the modulation is not readily extracted from the transform plot, because the analyzing wavelet picks out a scale  $\zeta l$  where, for the Morlet wavelet adopted

here,  $\zeta \sim 1.2$ , but is not a precisely defined number. From the location in transform space of the persistent pattern, the period is  $\sim 1.6$  yr. We may use a discrete form of the inversion formula given in the last section to reconstruct that part of the signal corresponding to a particular range of dilations, and have done that for two juxtaposed bands in this case. Specifically, we have made cuts just longward in period of the persistent modulation, and just shortward in period of the shorter period signal that peaks in 1985. We have divided that band at a dilation that optimizes the separation of the two periodic components. Figure 5 shows the reconstructed signal in each of the two bands. There is some ‘leakage’ between bands near to the center of the time series, but the periodic character of the variations is evident. Fitting a sinusoid to the inner-decade in each case yields periods of 1.66 yr and 1.12 yr. (In the cosmological comoving frame of the source, these periods are 1.27 yr and 0.86 yr respectively.) The fact that the longer period activity is a stable modulation of the underlying flow is evident from its phase coherence. Figure 6 shows this oscillation, superposed on which is a sinusoid of period 1.66 yr, and with the second half the reconstructed variation folded back on itself. Figure 7 shows the sum of the reconstructed signals and a tapered boxcar average of the original data. (Recall that the transform removes a local average.) Although the earlier periodogram analysis failed to provide clear-cut evidence for periodicity because of a smearing of power between these two signals, clearly a substantial portion of the source variation is accounted for by the two periodic components.

We have made a similar reconstruction at 4.8 GHz, and for both of the two bands of dilation have computed the spectral index,  $\alpha$ , defined in the sense  $S(\nu) \propto \nu^{-\alpha}$ . (As this requires us to take the ratio of fluxes, which obviously is not meaningful for quantities that oscillate about a zero mean, for each of the two dilation bands we have computed  $\alpha$  from the fluctuating portion of the signal plus a tapered boxcar mean.) Figure 8 displays the varying spectral indices, the bounds of which remain within values typical for flat spectrum sources (Aller, Aller, & Hughes 1992), with the spectra being most self-absorbed ( $\alpha < 0$ ) when the flux is at its highest. This is of course consistent both with an increase in flux being associated with an increase in intrinsic opacity, or with an increase in flux being associated with an increased Doppler boost with concomitant decrease in rest frame frequency – and so an increase in opacity – corresponding to a given observational frequency. Thus the spectral behavior of the source components does not allow us to discriminate between models for the periodic variation, but is consistent with the obvious candidates: a modulation of the flow density or direction.

To look for corresponding variations in the optical data, we have used Rosemary Hill Observatory data kindly supplied by S. Clements. We have performed a wavelet analysis of optical waveband variations from  $\sim 1970$  to  $\sim 1990$ , a time period comparable to that

covered by the radio data. Some structure is seen in the transform coefficients at the longest time scales, but no periodicity is evident, in particular on scales of order 1 yr. Both the radio data and the available Rosemary Hill Observatory optical data time series are, of course, too short to probe the 12 yr time scale evident in the historical optical data.

## 4.2. Interpretation: A Shock-In-Jet Model

We believe that an effective way to account for the behavior of the transform is with a ‘shock in jet’ model (Blandford & Königl 1979; Marscher, Gear, & Travis 1992), in which a region of enhanced emission (the down stream flow of the shock) travels along an otherwise quiescent flow, bounded by the  $\tau = 1$  surface (behind which the flow is optically thick, and the radiated flux is negligible) and a region of severe adiabatic energy loss, which also contributes negligible flux. Both effects depend so sensitively on position within the source, that to a good approximation the quiescent flow can be regarded as ‘windowed’ within axial extent  $z_1 \leq z \leq z_2$ . The propagating shock displaces *part* of the quiescent jet emission, as required by the transform behavior.

Consider a quiescent jet with specific emissivity a function of distance  $z$  along the flow:

$$d\varepsilon_j = z^{-\chi} dz; \quad z_1 \leq z \leq z_2, \quad (11)$$

along which a shock propagates with emissivity enhancement  $f$ :

$$d\varepsilon_s = f \times z^{-\chi} dz; \quad z_A(t) \leq z \leq z_B(t). \quad (12)$$

Within any segment of the flow the total emission is

$$\begin{aligned} \varepsilon^i &= \int_{z_{lo}}^{z_{hi}} [f] z^{-\chi} dz \\ &= [f] \frac{z^{-\chi+1}}{-\chi+1} \Big|_{z_{lo}}^{z_{hi}} \end{aligned} \quad (13)$$

where the factor  $f$  appears if this segment is within a shock. For example, when the shock is wholly within the windowed portion of the flow, we compute the total emission from the three segments:  $z_1 \leq z \leq z_A$ ,  $z_A \leq z \leq z_B$  and  $z_B \leq z \leq z_2$ . Now suppose that the emission is sinusoidally modulated, with slightly different frequencies in the quiescent and shocked portions. As the transform subtracts a mean, we need consider only the fluctuating portion of the signal, and observe

$$\varepsilon_{tot} = \sum_i \varepsilon_j^i(t) \sin(2\pi\nu_j t) + \varepsilon_s^i(t) \sin(2\pi\nu_s t). \quad (14)$$

We adopt a simple model for the evolution:

$$z_A = z_0(t) - \frac{\Delta}{2}; \quad z_B = z_0(t) + \frac{\Delta}{2}; \quad \Delta = \frac{1}{2}(z_2 - z_1) \quad (15)$$

where

$$z_0(t) = [3(z_2 - z_1)] \left[ \frac{t}{t_{\max}} \right] + (2z_1 - z_2). \quad (16)$$

This describes a component propagating with constant speed, and, with appropriate choice of  $z_1$  and  $z_2$ , of such a size as to provide ‘activity’ with the observed duration as a fraction of the whole time series. From the wavelet transform we know that  $\nu_j = 0.60 \text{ yr}^{-1}$  and  $\nu_s = 0.89 \text{ yr}^{-1}$ . It is possible that this difference originates from the different Doppler factors associated with these flow segments, there being an underlying frequency  $\nu_0$  Doppler contracted to  $\nu_0/\mathcal{D}_j$  in the case of the quiescent jet, and contracted to  $\nu_0/\mathcal{D}_s$  in the case of the shock. Another possibility is that different physical conditions in jet and shock lead to different natural frequencies for the development of oscillations. Values of other parameters that provide a good fit to the data are  $z_1 = 1$  and  $z_2 = 10$  and  $\chi = 1.5$ ,  $f = 3.5$ .

Figure 9 shows the Morlet transform of the model signal, which displays the main characteristics of the data transform. The model assumes a single event in the 1980s, whereas that activity might be due to any number of closely spaced structures with enhanced emissivity. The key point is that any activity with the general character adopted for the model can account for the evolution seen in transform space, and so provides support for a persistent modulation of an underlying flow.

The origin of this persistent modulation is unknown, but seems unlikely to be related simply to a helical bulk flow (e.g., Steffen et al. 1995; Vicente, Charlot, & Sol 1996), perhaps induced by precession of the central engine: the only way that helicity alone could produce a modulation of the emissivity is if a propagating structure has its instantaneous velocity vector directed periodically towards the observer as the structure traverses consecutive turns of the helix; but that would require a single event to persist for many turns, for several decades of time. The inevitable rotation of the outflow resulting from an accretion structure wind or magnetic torque (Wiita 1991) is not sufficient to explain the observations, as this does not break cylindrical symmetry. It is more likely that a disturbance drives a wave along the jet, so that the velocity vector of any comoving volume of jet material describes a helical trajectory due to its combined forward (axial) motion and a cyclical, transverse (precessional-like) motion. The velocity vector associated with the fixed, visible length of the flow – ‘windowed’ by opacity near to the core, and by severe adiabatic energy loss away from the core – will shift cyclically, and persistently, as does the thread of a screw at the surface through which it is being driven. This may be a manifestation of the Kelvin-Helmholtz instability: in principle, the surface helical

mode just introduces a cyclic transverse motion with the amplitude related to the angular frequency and the amplitude of the helical twist; body and higher order modes will be more complicated but all imply some precession of the velocity vector (P. Hardee, private communication). The modulation has a periodicity similar, but not identical, to the 1.2 yr value discussed by Katz (1997) as due to a ‘nodding’ of a precessing structure, but it is not obvious how such a motion would influence a jet.

Recently published VLBI images of OJ 287 (Gabuzda & Cawthorne 1996) show components typically from 1 to 7 pc from the core (assuming  $q_0 = 0.5$  and  $H_0 = 75 \text{ km s}^{-1} \text{ Mpc}^{-1}$ ). If we take 5 pc as a typical knot distance, and assume a flow opening angle of  $1^\circ$  (Marscher 1987; Muxlow & Garrington 1991), the radius of the flow at that point is  $\sim 0.05$  pc. The flow cannot rotate faster than the internal sound speed, and if that is  $c/\sqrt{3}$  – assuming a relativistic plasma – the rotation time will be  $\geq 1.5$  yr. It seems more plausible that a rotation of the flow would occur more slowly, but the bulk of the flux will probably be associated with the vicinity of the innermost knot, reducing the characteristic length scale, and permitting a rotation time as short as years. If this is, indeed, the explanation for the observed modulation, the latter is due to a nonrelativistic pattern, and would not be Doppler contracted. In that case, the different periodicities associated with jet and shock would reflect different internal states, and thus different phase speeds for wave propagation.

### 4.3. Constraints on Angle and Speed of Flow

We have noted that the different frequencies evident in the wavelet transform might reflect a single intrinsic frequency of modulation, Doppler contracted by different amounts in different segments of the flow. If that is so, we can use the ratio of frequencies to constrain aspects of the source dynamics; conversely, we can ask whether in the context of a ‘shock-in-jet’ model it is plausible that the observations are explained in this way. For a flow of speed  $\beta$  and Lorentz factor  $\gamma$ , viewed at angle  $\theta$  to the flow axis, the Doppler factor is

$$\mathcal{D} = \frac{1}{\gamma(1 - \beta \cos \theta)}. \quad (17)$$

Time scales are contracted by this amount, so that for flows modulated at a period  $P_0$ , but contracted to periods  $P_1$  or  $P_2$

$$\mathcal{R} = \frac{\mathcal{D}_2}{\mathcal{D}_1} = \frac{P_1}{P_2}. \quad (18)$$

If  $P_1$  and  $P_2$  are the periods of the persistent, jet flow, and the enhanced, perhaps shocked flow respectively,  $\mathcal{R} = 1.48$ .

Suppose first that the flow speed is unchanged, and that the change in Doppler factor arises solely from a change in flow orientation,  $\theta \rightarrow \theta + \Delta\theta$ . If  $|\Delta\theta| \ll 1$  then using the apparent speed

$$\beta_a = \frac{\beta \sin \theta}{1 - \beta \cos \theta}, \quad (19)$$

we may write

$$1 + \beta_a \Delta\theta = \mathcal{R}^{-1}, \quad (20)$$

where we interpret  $\Delta\theta$  as the change from the initial flow to enhanced flow phase. With the caveat that knots may represent a pattern speed, and not the speed of the underlying flow, we can use the observed superluminal motion of OJ 287 (Gabuzda & Cawthorne 1996; Gabuzda, Wardle, & Roberts 1989) to estimate that  $\beta_a \sim 4.4$ , for the cosmological parameters adopted (see above). This value was measured in the early 1980s, and is therefore indeed appropriate to the initial flow. Moreover, there is only a modest dispersion in the apparent speeds measured for the three components visible in the 1980s, justifying the use of a single value throughout the time of interest. From the values of  $\beta_a$  and  $\mathcal{R}$  we have  $\Delta\theta = -4.2^\circ$ . Thus, a fairly modest change in flow direction is sufficient to explain the change in Doppler factor necessary to account for the change in observed periodicity. For a flat spectrum source in which the enhanced emission fills the observable ‘window’ of the flow – to a first approximation – the observed flux will be increased by the increased Doppler boost,  $\mathcal{B} \approx \mathcal{D}^2$ , which implies a flux increase by a factor of  $\sim 2.2$ ; this could certainly account for much of the brightening observed in the 1980s. The primary reason for discounting this scenario is that as the shorter and longer period signals coexist at some epochs, and as hints of the shorter period signal are evident at late epochs, we would require that only a portion of the flow reorients itself by  $\sim 4^\circ$ , and then most but not all of that flow segment relaxes back to its original configuration. Furthermore, the scenario is implausible because we would expect a continuous range of viewing angles for a curved flow, not the essentially bimodal distribution necessary to produce two distinct periods.

The obvious alternative scenario is that the flow speed changes:  $\beta \rightarrow \beta + \Delta\beta$ ,  $\gamma \rightarrow \gamma + \Delta\gamma$ , where  $\Delta\gamma = \beta\gamma^3\Delta\beta$ . Consider such a change, in which the flow orientation is fixed. As before, we can write

$$1 - (\gamma\mathcal{D} - \gamma^2) \left( \frac{\Delta\beta}{\beta} \right) - (\gamma\mathcal{D} - 1) \gamma^2 \beta^2 \left( \frac{\Delta\beta}{\beta} \right)^2 = \mathcal{R}^{-1}. \quad (21)$$

If we are viewing close to the critical cone of the flow, then  $\mathcal{D} \sim \gamma \sim \beta_a$ , so that the second term of the previous expression is negligible, and

$$\Delta\beta = \left[ \frac{1 - \mathcal{R}^{-1}}{(\beta_a^2 - 1) \beta_a^2} \right]^{1/2}. \quad (22)$$

Using our previous parameter values, we find that  $\Delta\beta = 0.03$ , while the corresponding (arithmetic) change in Lorentz factor is  $\Delta\gamma = 2.6$ . The inferred  $\Delta\beta/\beta$  is barely small enough to justify the simple linearization used above, but the numbers are certainly illustrative of the change required. A change of  $\gamma$  from 4.4 to  $\sim 7$  requires a Lorentz transformation by only  $\gamma \sim 1.1$ , consistent with the result that much source activity can be explained by weak shocks (Jones 1988).

## 5. Analysis of the Polarized Flux Variations

### 5.1. The Transform Coefficients

A wavelet analysis identical to that applied to the total flux has been used to explore variations in the polarized flux. We have made separate studies of the  $Q$  and  $U$  Stokes parameters, and Figure 10 displays the signal and transform coefficients for 14.5 GHz  $U$  data for OJ 287. The same persistent signal as seen in the total flux is evident here. The influence of mid-1980s activity is barely apparent, which may be explained by the ‘enhanced flux’ component being more opaque, and contributing little to the polarized flux; however, as we discuss below, there is evidence for a change in character of the polarized fluctuations at this time. A longer period signal is also apparent – just above the lower edge of the plot of the real part of the transform, during the 1980s – which may be more evident in the polarized flux than in the total flux, because optically thin, and thus probably more extended, structures will tend to dominate the polarization. This possible longer period signal cannot be explored with a time series of several decades in length, and we do not discuss it further. The transform of  $Q$  also displays the longer period signal, but the persistent 1.66 yr signal is almost absent, indicating that the fluctuations are almost entirely in  $U$ . The transforms at 8.0 and 4.8 GHz are very similar to that at 14.5 GHz.

Examination of  $Q$ - $U$  plots for the other two observing frequencies shows a similar pattern of behavior, but with different orientation to the axis of variations. We have explored this by computing transforms for both  $Q$  and  $U$ , with the  $Q$ - $U$  plane systematically rotated, in each case looking to see what rotation maximizes the variations in  $U$ . As a measure of the variations, we have integrated the reconstructed fluctuating signal over all times (translations). At 14.5 GHz a rotation of  $-12^\circ$  was needed to maximize  $U$ , while at 8.0 and 4.8 GHz the angles were found to be  $0^\circ$  and  $30^\circ$  respectively. This serves to quantify the degree to which variations relate to the VLBI jet directions, but also suggests a systematic variation with frequency that may be due either to the presence of a Faraday medium, or to the fact that at different observing frequencies, observations are sensitive to different parts of the flow, i.e., the  $\tau = 1$  surface moves inwards at higher frequency.

We have reconstructed the periodic part of the signal, using the range of dilations adopted for the total flux, for both  $Q$  and  $U$ , and Figure 11 displays the evolution of this signal at 14.5 GHz for the longer period of the two bands adopted earlier. Note that as the transform removes the mean, the points are placed about the origin of the plane. To provide a more meaningful indication of  $Q$ - $U$  plane evolution, we have computed a tapered boxcar average of the original signal, and in Figure 12 show the sum of this and the fluctuating part. The evolution is most easily seen when displayed dynamically (an animation is available at the primary author’s WWW site: <http://www.astro.lsa.umich.edu/users/hughes/>), and has the character of smooth ‘orbits’ about the origin. Looking only at the modulated component (Figure 11) we see that the source oscillates in the  $Q$ - $U$  plane, initially along an axis approximately coincident with the direction of the VLBI jet ( $-110^\circ$ ; Gabuzda & Cawthorne 1996), but thereafter along an axis orthogonal to that, until the variations fall back to their original character towards the mid-1990s. As will be demonstrated in the next section, the smoothness of variation is an artifact of the filtering: by reconstructing the signal from a limited range of dilations, the short period fluctuations that normally endow  $Q$ - $U$  plots with a highly irregular character have been removed. Nevertheless, the analysis does highlight that during the activity of the 1980s the polarized flux varied almost entirely in  $U$ , which given the jet orientation, corresponds to ‘excursions’ of the electric vector about  $45^\circ$  to the flow axis.

Examination of Figure 12 shows that at early epochs, the polarized flux was primarily in  $-Q$ , corresponding to an electric vector orthogonal to the VLBI flow, while during the more active phase that follows, a significantly fluctuating electric vector more closely aligned with the flow occurs. This is qualitatively consistent with a picture in which an axial magnetic field gives way to a transverse field during activity – as envisaged by the standard ‘shock-in-jet’ models (Hughes, Aller, & Aller 1985, 1989) – but with the effective field orientation modulated by a corkscrew-like wave of the internal velocity vector of the flow as discussed above, with further complexity perhaps added by the effects of relativistic aberration.

The relationship between the variations in  $I$  and those in  $U$  is somewhat complicated, but the trends may be exposed by comparing and combining the reconstructed signals from both the low and high frequency dilation bands. Figure 13 shows the cross-correlation function of  $I$  and  $U$  variations in the low frequency band. The correlation function behaves in a manner very similar to that expected from two sinusoidal signals, which are out of phase by  $\pi$ , leading to a strong anticorrelation at zero lag. Such behavior is evident from Figure 14, which shows the product of these two signals. The broken horizontal line near to the top of the plot marks where the two signals have the same sign. Although there are epochs that run counter to this trend, as a general rule the  $I$  and  $U$  signals are

anticorrelated. A similar analysis of the high frequency band shows the same general trends. This is clearly an aspect of the data that must be explained by any detailed model for the behavior discussed here, and such a model is outside the scope of this paper, as it demands calculation of the effects of aberration and projection for particular possible flow patterns.

## 5.2. Interpretation: Comparison With a Random Walk Model

It has been known since observations of polarization rotations in the UMRAO data and subsequent interpretation by Jones et al. (1985) in terms of a random walk model, that the turbulent character of the magnetic field in sources such as BL Lacs plays a major role in determining their polarization behavior. In this view, the source is composed of a number of randomly aligned magnetic field elements, the polarized emissions from which add to yield a small but non-zero net polarized flux. The flow advects these ‘cells’ of magnetic field, so that new cells enter through the  $\tau = 1$  surface, as others are lost to view in the adiabatically-expanded outer regions of the flow. Thus, at close times, a subset of cells have changed, but a substantial number are common to the two epochs, leading to a coherence in the stochastically varying net polarization.

Rotations arise because once at an extremum in the  $Q-U$  plane, the subsequent evolution must by definition have some component towards the origin, and the coherence of the process guarantees that once a source evolves in that direction, it will continue to do so for some further time. In general, the  $Q-U$  plane locus will pass some distance from the origin, and eventually do so again at some other polarization angle, having effectively rotated in  $Q-U$ . Can this effect explain the evolution of the periodic part of the polarized flux just described? We have constructed a simple model, in which unit vectors are randomly aligned, and a net polarized flux was computed assuming that each cell contributes the same absolute value. Our model employs 100 cells, 5 of which are replaced by new ones at each of 750 time steps. The resultant behavior of  $U$  is superficially similar to that seen in OJ 287; however, this is misleading.

Figure 15 displays the evolution of a portion of the  $Q$  and  $U$  signals, reconstructed from a wavelet transform of the mock signals. The smoothness results from the filtering – the original  $Q-U$  plane evolution is much more erratic. A particular direction in this plane appears to have been picked out, but that arises from the modest number of excursions in the plane: small number statistics cause a chance alignment of these loops. In particular, the excursions are randomly aligned with time, there being no tendency to repeatedly move along a specific orientation, *unlike the variations seen in OJ 287, where during the distinct activity of the 1980s, the  $Q-U$  plane excursions are consistently in the same direction.* We

conclude that such a random walk model cannot explain the character of the modulated polarization behavior seen in the OJ 287 data.

## 6. Discussion

We have found that a continuous wavelet transform of the multifrequency, total flux and polarization data for the BL Lac object OJ 287 clearly reveals a periodicity that is merely hinted at by a more conventional Fourier analysis. The modulation of the total flux persists for the duration of the time series available, but changes its period in the 1980s in a way that is consistent with the kinematics of a ‘shock-in-jet’ model, wherein a portion of a previously quiescent flow is replaced by a propagating domain of enhanced emissivity. This may be a single event, or a series of closely-spaced individual events. In either case, the modulation appears to be an additional phenomenon, superposed on longer-term trends, and may be a consequence of a precessional-like motion of the flow in the vicinity of the  $\tau = 1$  surface, as a consequence of propagating modes of the Kelvin-Helmholtz instability. Such behavior is evident also in the polarized flux, for which the most notable feature is a series of periodic excursions along a well-defined axis in the  $Q-U$  plane which is at about  $45^\circ$  from the direction defined by the VLBI jet. This behavior differs in detail from what would be expected from a ‘random walk’ model, and it also is suggestive of a periodic variation in the direction of the jet, and its mean magnetic field component, at that point along the flow from which most of the emission originates in the cm-waveband.

Detailed modelling is called for to explore this behavior, but will require that allowance be made for projection and relativistic aberration effects. As the latter will be determined by the details of the flow’s velocity field, it will be interesting to see if the observed behavior can be a generic feature of unstable flows, or requires finely-tuned geometry, magnetic field topology and velocity distribution.

Were OJ 287 to be in an radio-active phase, intensive, space-based monitoring of the evolution of VLBI components recently ejected from the core would provide potentially exciting data, because such a component would define the detailed kinematics of the flow that dominates the total flux data. Unfortunately, as evidenced by UMRAO monitoring, the source is in a protracted quiescent phase, and further understanding of this object may have to await renewed activity.

A possibility worth exploration is that OJ 287 is not unique amongst well-observed sources, but merely a source with particularly short time scale periodic components. It may well be that some long term variations seen in other sources are manifestations of a similar

modulation, but expressed in those sources in a far less evident and accessible way: the UMRAO database is not temporally long enough to easily identify such behavior. We plan to explore other sources of the UMRAO database, in an attempt to identify similar activity through signatures such a phase coherence of outbursts over long times scales.

This research was supported in part by grants AST-9421979 and AST-9617032 from the National Science Foundation. We wish to thank Denise Gabuzda for comments that helped us improve the presentation of this material.

## REFERENCES

- Aller, M. F., Aller, H. D., & Hughes, P. A. 1992, *ApJ*, 399, 16
- Aller, M. F., Aller, H. D., & Hughes, P. A. 1994, in *Workshop on Intensive Monitoring of OJ 287*, ed. M. R. Kidger & L. O. Takalo (Turku: Tuorla Observatory), 60
- Aller, M. F., Aller, H. D., Hughes, P. A., & Latimer, G. E. 1992, in *Variability of Blazars*, ed. E. Valtaoja & M. Valtonen (Cambridge: Cambridge Univ. Press), 126
- Aller, H. D., Aller, M. F., Latimer, G. E., & Hodge, P. E. 1985, *ApJS*, 59, 513
- Aller, H. D., Aller, M. F., Latimer, G. E., & Hughes, P. A. 1997, in preparation
- Birkinshaw, M. 1991, in *Beams and Jets in Astrophysics*, ed. P. A. Hughes (Cambridge: Cambridge Univ. Press), 278
- Blandford, R. D., & Königl, A. 1979, *ApJ*, 232, 34
- Boltwood, P. 1996, in *Workshop on Two Years of Intensive Monitoring of OJ 287 and 3C 66A*, ed. L. O. Takalo (Turku: Tuorla Observatory), 50
- Bregman, J. N. 1994, in *Multi-wavelength Continuum Emission of AGN*, ed. T.J.-L. Courvoisier & A. Blecha (Dordrecht: Kluwer), 5
- Carrara, E. A., et al. 1993, *A&A*, 279, 83
- Cawthorne, T. V., & Wardle, J. F. C. 1988, *ApJ*, 332, 696
- Deeming, T. J. 1975, *Ap&SS*, 36, 137
- Farge, M. 1992, *Ann. Rev. Fluid Mech.*, 24, 395
- Gabuzda, D. C., & Cawthorne, T. V. 1996, *MNRAS*, 283, 759
- Gabuzda, D. C., Wardle, J. F. C., & Roberts, D. H. 1989, *ApJ*, 336, L59
- Haykin, S., & Kesler, S. 1979, in *Nonlinear Methods of Spectral Analysis*, ed. S. Haykin (Berlin: Springer-Verlag), 9
- Hughes, P. A., Aller, H. D., & Aller, M. F. 1985, *ApJ*, 298, 301
- Hughes, P. A., Aller, H. D., & Aller, M. F. 1989, *ApJ*, 341, 68
- Hughes, P. A., Aller, H. D., & Aller, M. F. 1991, *ApJ*, 374, 57
- Hughes, P. A., Aller, H. D., & Aller, M. F. 1992, *ApJ*, 396, 469
- Icke, V. 1991, in *Beams and Jets in Astrophysics*, ed. P. A. Hughes (Cambridge: Cambridge Univ. Press), 232
- Jenkins, G. M., & Watts, D. G. 1968, *Spectral Analysis and Its Applications*, (Oakland: Holden-Day)

- Jones, T. W. 1988, *ApJ*, 332, 678
- Jones, T. W., Rudnick, L., Aller, H. D., Aller, M. F., Hodge, P. E., & Fiedler, R. L. 1985, *ApJ*, 290, 627
- Katz, J. I. 1997, *ApJ*, 478, 527
- Kidger, M. R., & González-Pérez, J. N. 1994, in *Workshop on Intensive Monitoring of OJ 287*, ed. M. R. Kidger & L. O. Takalo (Turku: Tuorla Observatory), 49
- Marscher, A. P. 1987, in *Superluminal Radio Sources*, ed. J. A. Zensus & T. J. Pearson (Cambridge: Cambridge Univ. Press), 280
- Marscher, A. P. 1993, in *Sub-arcsecond Radio Astronomy*, ed. R. J. Davis & R. S. Booth (Cambridge: Cambridge Univ. Press), 297
- Marscher, A. P., Gear, W. K., & Travis, J. P. 1992, *Variability of Blazars*, ed. E. Valtaoja & M. Valtonen (Cambridge: Cambridge Univ. Press), 85
- Miller, J. S., French, H. B., & Hawley, S. A. 1978, in *Pittsburgh Conference on BL Lac Objects*, ed. A. M. Wolfe (Pittsburgh: University of Pittsburgh), 176
- Mutel, R. L., Phillips, R. B., Su, B., & Bucciferro, R. R. 1990, *ApJ*, 352, 81
- Muxlow, T. W. B., & Garrington, S. T. 1991, in *Beams and Jets in Astrophysics*, ed. P. A. Hughes (Cambridge: Cambridge Univ. Press), 52
- Scargle, J. D. 1982, *ApJ*, 263, 835
- Sillanpää, A., Haarala, S., Valtonen, M. J., Sundelius, B., & Byrd, G. G. 1988, *ApJ*, 325, 628
- Sillanpää, A., et al. 1994, in *Workshop on Intensive Monitoring of OJ 287*, ed. M. R. Kidger & L. O. Takalo (Turku: Tuorla Observatory), 7
- Sitko, M. L., & Junkkarinen, V. T. 1985, *PASP*, 97, 1158
- Steffen W., Zensus J. A., Krichbaum T. P., Witzel A., & Qian S. J. 1995, *A&A*, 302, 335
- Ulrych, T. J., & Ooe, M. 1979, in *Nonlinear Methods of Spectral Analysis*, ed. S. Haykin (Berlin: Springer-Verlag), 73
- Valtaoja, E., Teräsanta, H., & Tornikoski, M. 1994, in *Workshop on Intensive Monitoring of OJ 287*, ed. M. R. Kidger & L. O. Takalo (Turku: Tuorla Observatory), 55
- Valtonen, M. J., & Lehto, H. J. 1997, *ApJ*, 481, L5
- Vicente, L., Charlot, P., & Sol, H. 1996, *A&A*, 312, 727

Wiita, P. J. 1991, in *Beams and Jets in Astrophysics*, ed. P. A. Hughes (Cambridge: Cambridge Univ. Press), 379

Fig. 1.— 30 day averaged data for OJ 287. The bottom panel is total flux, the middle panel polarized flux, and the top panel is the position angle of the polarization vector ( $E$ -field). Triangles denote 4.8 GHz data, circles 8.0 GHz data, and crosses 14.5 GHz data.

Fig. 2.— Morlet transforms of a. Gaussian white noise; b. a sinusoid in which the frequency halves at the mid-point of the time series. The top panel is the signal, the second panel is the real part of the transform coefficients, the third panel is the coefficient modulus, and the fourth panel is the phase. There is a one-to-one correspondence between epochs in the time series and those in the transform space; dilation increases from top to bottom in each panel. Panels two through four are color-coded with the minimum value shown as blue, and maximum value shown as red.

Fig. 3.— A Morlet transform for 14.5 GHz total flux data for the source OJ 287. The panels are as described for Figure 2. The two ‘bands’ discussed in the text are indicated by vertical bars to the right of the panel displaying the real part of the transform.

Fig. 4.— Morlet transforms of a. BL Lac at 14.5 GHz; b. NRAO 140 at 14.5 GHz. The panels are as described for Figure 2, although the phase is not shown.

Fig. 5.— The reconstructed signal from the transform of 14.5 GHz data for OJ 287. The upper panel is for the band of dilations that picks out the shorter period activity most prominent in the 1980s, while the lower panel picks out the persistent 1.66 yr activity.

Fig. 6.— The longer period signal from Figure 5 (lower panel), shown as a solid line, with the second half of this signal folded back on itself to show the phase coherence (dashed line) and a sinusoid of period 1.66 yr superposed (dotted line).

Fig. 7.— The sum (solid line) of the two reconstructed signals (Figure 5) for 14.5 GHz OJ 287 data, added to a tapered boxcar average of the original data (dotted line).

Fig. 8.— The 4.8 GHz–14.5 GHz spectral index for the two reconstructed signals (Figure 5) for 14.5 GHz OJ 287 data: longer period signal (dotted); shorter period signal (dashed).

Fig. 9.— A Morlet transform for the ‘shock-in-jet’ model signal. The panels are as described for Figure 2, although the phase is not shown.

Fig. 10.— A Morlet transform for 14.5 GHz  $U$  data for the source OJ 287. The top panel is the signal, the second panel is the real part of the transform coefficients, the third panel is the coefficient modulus. Panels two and three are color-coded with the minimum value shown as blue, and maximum value shown as red.

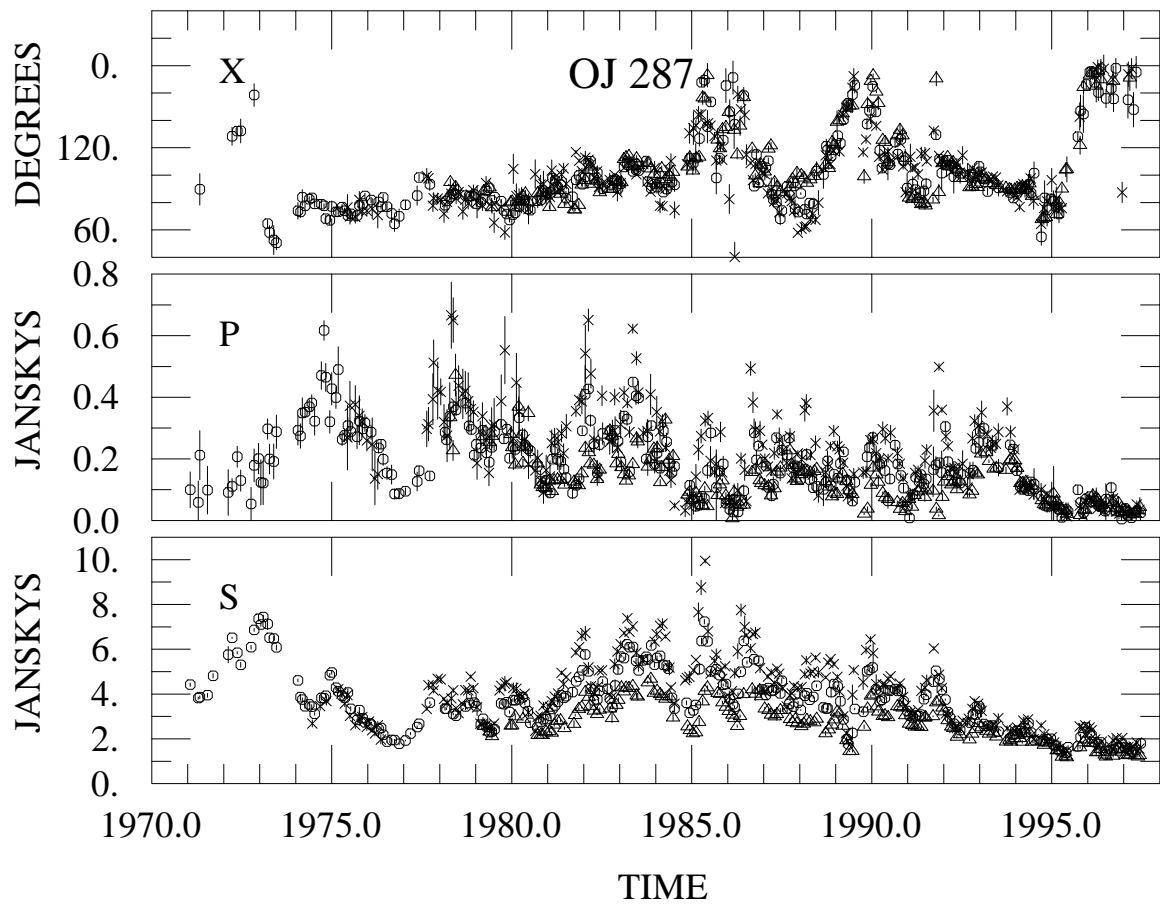
Fig. 11.— Evolution in the  $Q$ - $U$  plane of the periodic part of the 14.5 GHz OJ 287 polarized flux.

Fig. 12.— As for Figure 11, but with a tapered boxcar average added to give a more instructive view of  $Q$ - $U$  plane evolution.

Fig. 13.— The cross-correlation function for  $I$  and  $U$  in the ‘low frequency’ band of the wavelet transform of OJ 287 at 14.5 GHz.

Fig. 14.— The product of the  $I$  and  $U$  ‘low frequency’ band variations from the wavelet transform of OJ 287 at 14.5 GHz. The line near to the top of the plot marks times when the two signals have the same sign.

Fig. 15.—  $Q$ - $U$  plane evolution for the filtered random walk model.



This figure "figure2a.gif" is available in "gif" format from:

<http://arxiv.org/ps/astro-ph/9802275v1>

This figure "figure2b.gif" is available in "gif" format from:

<http://arxiv.org/ps/astro-ph/9802275v1>

This figure "figure3.gif" is available in "gif" format from:

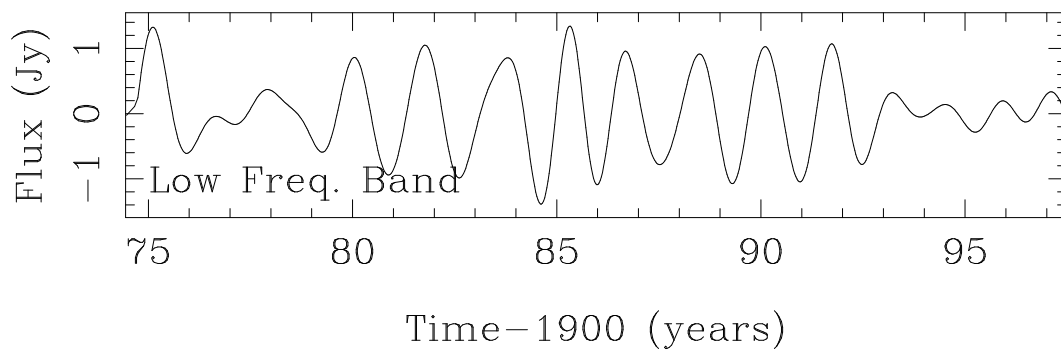
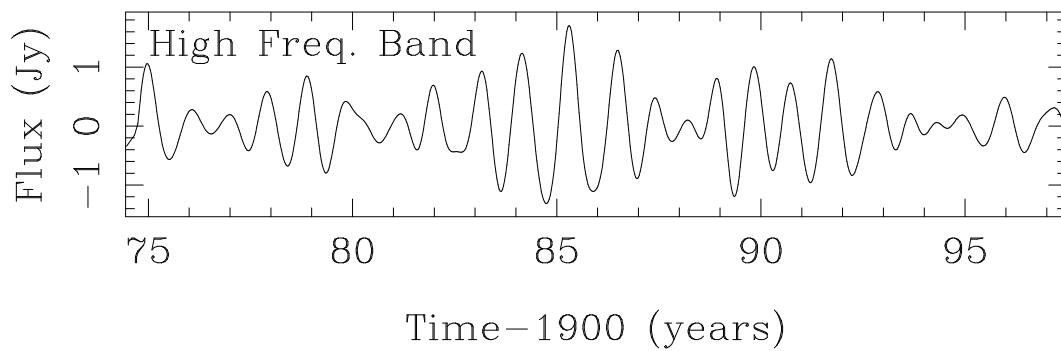
<http://arxiv.org/ps/astro-ph/9802275v1>

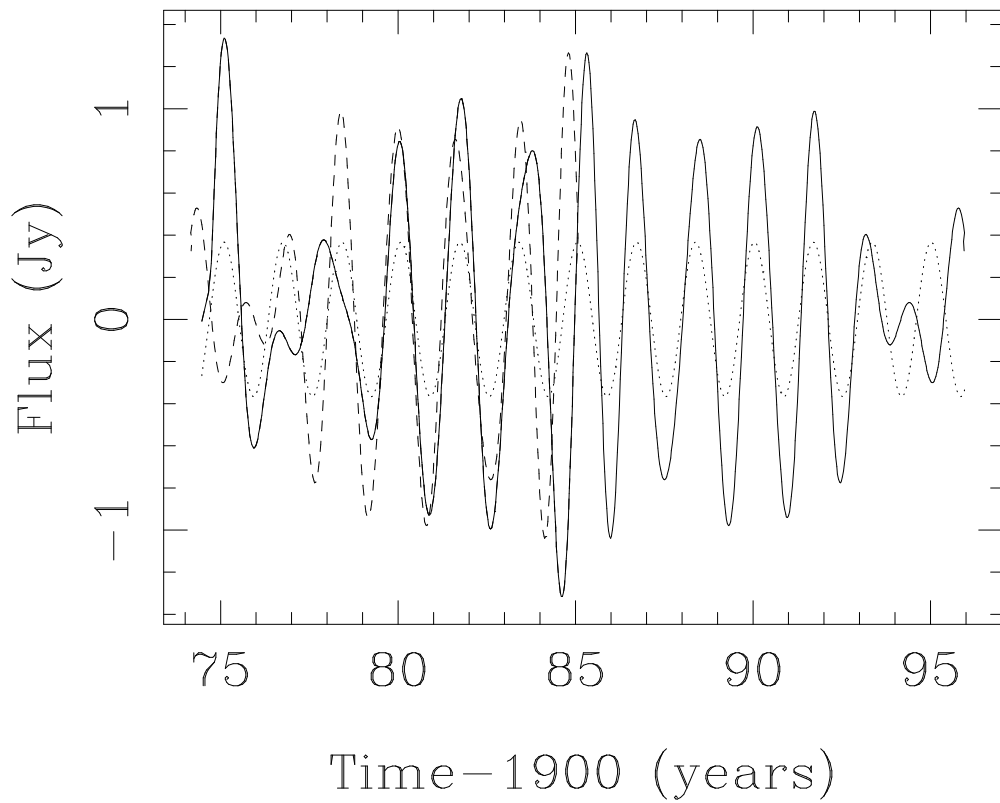
This figure "figure4a.gif" is available in "gif" format from:

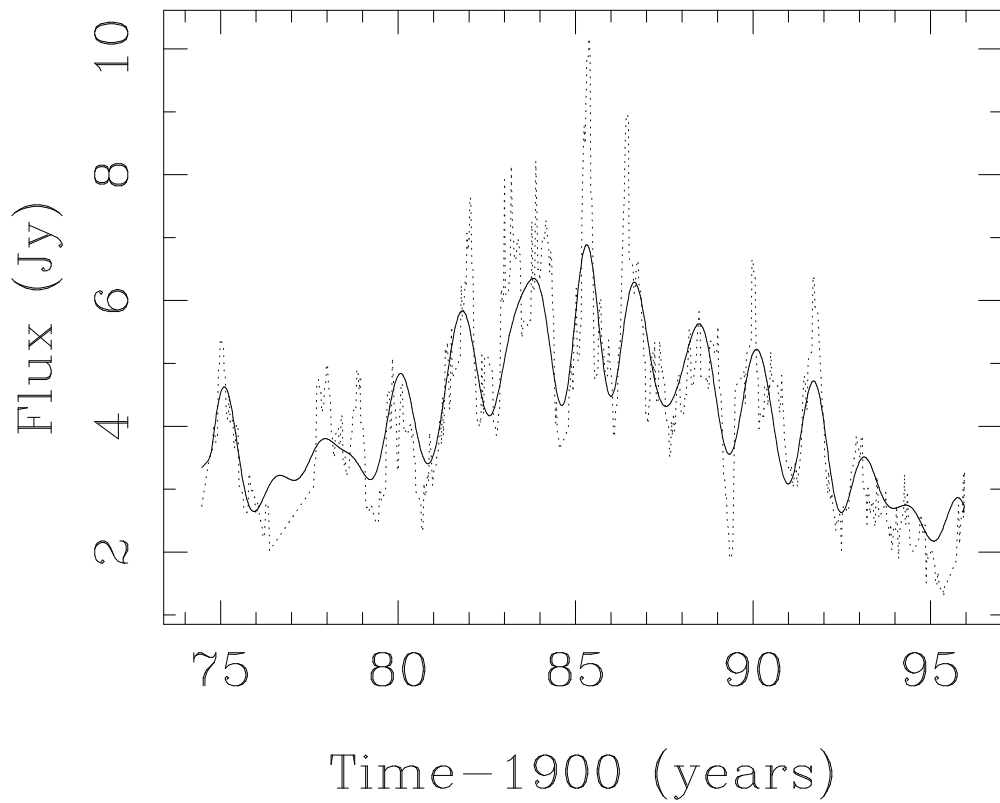
<http://arxiv.org/ps/astro-ph/9802275v1>

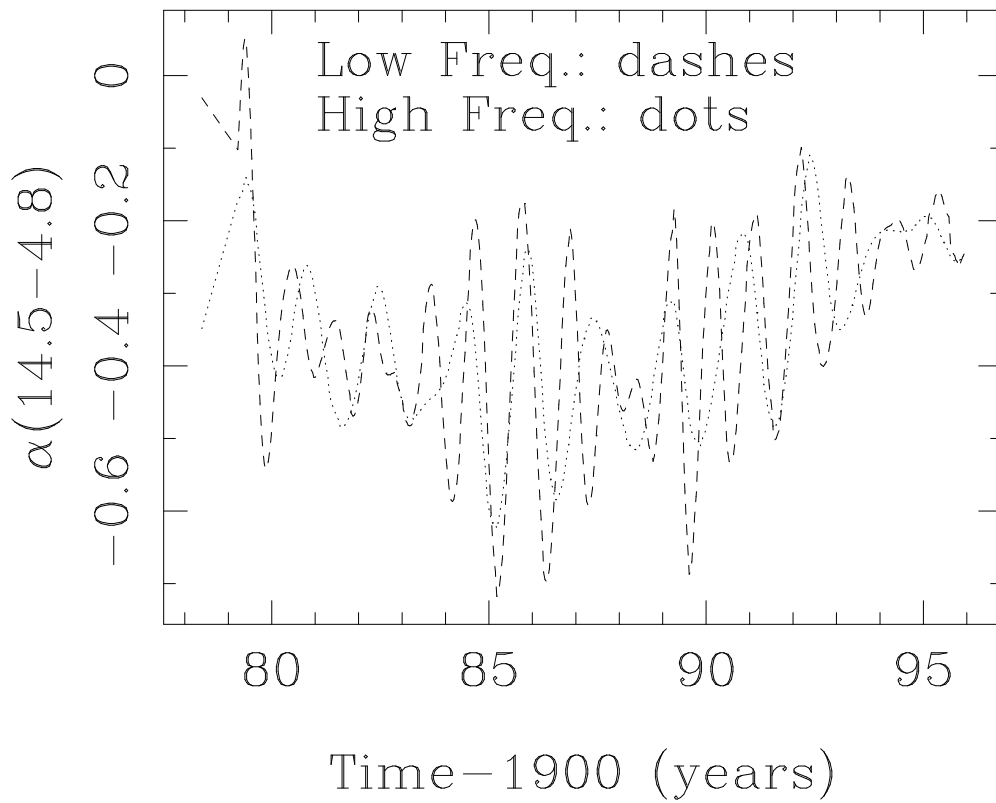
This figure "figure4b.gif" is available in "gif" format from:

<http://arxiv.org/ps/astro-ph/9802275v1>









This figure "figure9.gif" is available in "gif" format from:

<http://arxiv.org/ps/astro-ph/9802275v1>

This figure "figure10.gif" is available in "gif" format from:

<http://arxiv.org/ps/astro-ph/9802275v1>

